

Article

Microwave-Assisted Synthesis, Optical and Theoretical Characterization of Novel 2-(imidazo[1,5-*a*]pyridine-1-yl)pyridinium Salts

Luca M. Cavinato ¹, Giorgio Volpi ^{2,*}, Elisa Fresta ¹, Claudio Garino ², Andrea Fin ³ and Claudia Barolo ²

- ¹ Chair of Biogenic Functional Materials, Technical University of Munich, Schulgasse 22, 94315 Straubing, Germany; luca.cavinato@tum.de (L.M.C.); elisa.fresta@tum.de (E.F.)
- ² Department of Chemistry, University of Turin, Via Pietro Giuria 7, 10125 Turin, Italy; claudio.garino@unito.it (C.G.); claudia.barolo@unito.it (C.B.)
- ³ Department of Drug Science and Technology, University of Turin, Via Pietro Giuria 9, 10125 Turin, Italy; andrea.fin@unito.it
- * Correspondence: giorgio.volpi@unito.it

Abstract: In the last few years, imidazo[1,5-*a*]pyridine scaffolds and derivatives have attracted growing attention due to their unique chemical structure and optical behaviors. In this work, a series of pyridylimidazo[1,5-*a*]pyridine derivatives and their corresponding pyridinium salts were synthesized and their optical properties investigated to evaluate the effect of the quaternization on the optical features both in solution and polymeric matrix. A critical analysis based on the spectroscopic data, chemical structures along with density functional theory calculation is reported to address the best strategies to prevent aggregation and optimize the photophysical properties. The obtained results describe the relationship between chemical structure and optical behaviors, highlighting the role of pendant pyridine. Finally, the presence of a positive charge is fundamental to avoid any possible aggregation process in polymeric films.

Keywords: blue emitters; large stokes shift; microwave synthesis; thin film; imidazo[1,5-*a*]pyridine; acceptor small molecules



Citation: Cavinato, L.M.; Volpi, G.; Fresta, E.; Garino, C.; Fin, A.; Barolo, C. Microwave-Assisted Synthesis, Optical and Theoretical Characterization of Novel 2-(imidazo[1,5-*a*]pyridine-1-yl)pyridinium Salts. *Chemistry* **2021**, *3*, 714–727. <https://doi.org/10.3390/chemistry3030050>

Academic Editor: Radomir Jasinski

Received: 16 June 2021

Accepted: 1 July 2021

Published: 6 July 2021

Publisher's Note: MDPI stays neutral with regard to jurisdictional claims in published maps and institutional affiliations.



Copyright: © 2021 by the authors. Licensee MDPI, Basel, Switzerland. This article is an open access article distributed under the terms and conditions of the Creative Commons Attribution (CC BY) license (<https://creativecommons.org/licenses/by/4.0/>).

1. Introduction

Imidazo[1,5-*a*]pyridines are a promising family of fluorophores that can be easily functionalized to tune their photophysical properties, characterized by a high photoluminescent quantum yield (up to 50%) and a large Stokes shift (up to 150 nm) [1–4]. The synthetic feasibility via a one-pot cyclocondensation reaction, without the use of any metal catalyst or highly sensitive Lewis acid, has been previously demonstrated [5,6]. Furthermore, the derivatives of the imidazo[1,5-*a*]pyridine scaffold have been used both for building small molecules and as ligands for organometallic complexes [7–9], displaying promising performances in both cases. They have also been successfully implemented in numerous fields, such as chemical sensors [10], confocal microscopy [11,12], and medical applications [13,14]. Recently, imidazo[1,5-*a*]pyridinium salts have also been intensively investigated in particular as pH sensor [15,16], promising candidates in a photoactive component for Photodynamic Therapy (PDT) [17,18] and emissive helical cationic-type molecules [19]. Despite the large interest in these compounds, depicted by numerous works on the quaternization onto the imidazo[1,5-*a*]pyridine moiety in mono- or dimeric forms, a systematic study about the quaternization reaction onto pyridylimidazo[1,5-*a*]pyridine derivatives and their optical properties is still lacking. This is of utter importance as both pyridylimidazo[1,5-*a*]pyridine derivatives and their salts are gaining considerable interest for optoelectronic applications such as solution-processed light-emitting devices (OLEDs [20,21] and LECs [22,23]). In the latter field, two issues are particularly bothersome: the first is the lack of high-energy stable emitters, while the second one is the lack of sustainable ionic emitters [24–27]. Blue

light-emitting imidazo[1,5-*a*]pyridine derivatives are key to both problems as they are, *per se*, high-energy emitting and can be quaternized in a straight-forward manner. A common strategy to introduce a charged functional group involves anchoring of the imidazolium moiety through an alkyl chain to the imidazo[1,5-*a*]pyridine core and subsequently its quaternization [28–32]. This approach preserves the photophysical features of the core but presents some disadvantages. It can introduce electrochemical stability issues, it limits the selection of the host materials to the ones properly designed for OLED devices and it requires a Suzuki coupling step catalyzed by expensive and rare transition metals. The latter is in contrast with the low-cost and sustainable goals of the LEC technology.

Herein, we report a detailed optical and theoretical characterization of three archetypal pyridylimidazo[1,5-*a*]pyridine derivatives **1–3** and their quaternized salts **1q–3q**—Figure 1. This class of compounds is prone to aggregate in thin films with a dramatic loss of photoluminescence quantum yields, which affects their performance in electroluminescence devices [22]. Recently, Albrecht et al. [21] optimized the substitution of 1,3-disubstituted imidazo[1,5-*a*]pyridines and -quinolines in thin films and OLED devices, demonstrating the feasibility of obtaining electroluminescence from these fluorophores. This year, O. Y. Vassilyeva et al. [33] used imidazo[1,5-*a*]pyridinium-based cations and halometallate anions as fluorescent agents to ensure excellent dispersion of the luminescent components in a polymeric matrix and prevent solid-state quenching.

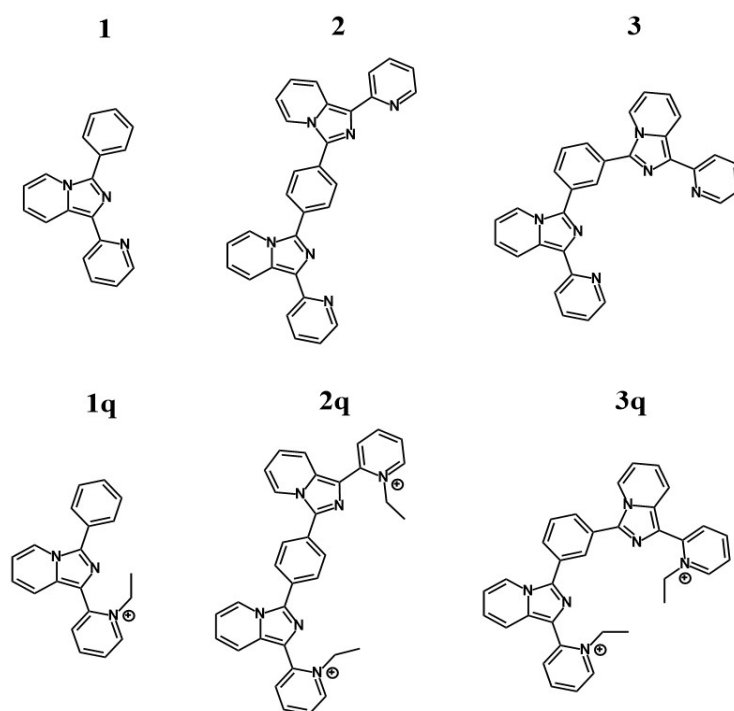


Figure 1. Structures of the molecules reported in this contribution.

Nevertheless, a complete characterization of photophysical behavior in both solution and thin films of a series of blue-emitters and their corresponding pyridinium salts is still lacking. This is of utter relevance to define strategies to rule out aggregation in the solid state. In this context, we provide a full study on the impact of both the introduction of double imidazo[1,5-*a*]pyridine moieties and charge sites, as well as on the impact of the quaternization on the photophysical features in both solution and thin film—Figure 1. This was performed on pristine thin films of the emitters and on emitters mixed with common polymeric matrices, giving highlights on the best strategies to reduce aggregation and retain optimal photophysical properties.

2. Materials and Methods

2.1. Synthesis

All chemicals and solvents were purchased and used without further purification. The reaction monitoring via thin-layer chromatography (TLC) was performed on silica gel TLC-PET foils GF 254, particle size 25 mm, medium pore diameter 60 Å (Honeywell Fluka™, Seelze, Germany). All reactions were carried out with a microwave-assisted protocol on a Biotage® Initiator (Uppsala, Sweden), the volume of the vials was between 0.2 and 20 mL.

The ^1H and ^{13}C NMR spectra were recorded on a JEOL Resonance 600 (^1H NMR operating frequency 600 MHz) at 298 K. All chemical shifts are relative to TMS ($\delta = 0$) and referenced against solvent residual peaks. The following abbreviations are used for the multiplicity: s (singlet), d (doublet), t (triplet), dd (doublet of doublets), dt (doublet of triplets), ddd (doublet of doublet of doublets), m (multiplet). The ^{13}C NMR of **2q** and **3q** are not reported due to solubility issues.

Mass spectra were recorded using an LCQ Advantage MAX Ion Trap Spectrometer (Thermo Fisher Scientific, Dreieich, Germany) equipped with an electrospray ion source (ESI).

2.1.1. Synthesis of 3-phenyl-1-(pyridin-2-yl)imidazo[1,5-*a*]pyridine (**1**)

Derivative **1** was synthesized as previously reported [34] (yield 83%, 1.3 g). Mass (ESI) m/z calculated for $\text{C}_{18}\text{H}_{13}\text{N}_3$ ($[\text{M} + \text{H}]^+$): 272.11; found: 272.06: ^1H NMR (600 MHz, Acetone- d_6) δ 8.71 (dt, $J = 9.2, 1.3$ Hz, 1H), 8.59 (ddd, $J = 4.8, 1.9, 0.9$ Hz, 1H), 8.45 (dt, $J = 7.1, 1.1$ Hz, 1H), 8.22 (dt, $J = 8.0, 1.1$ Hz, 1H), 7.94–7.88 (m, 2H), 7.76 (ddd, $J = 8.0, 7.4, 1.8$ Hz, 1H), 7.60–7.52 (m, 2H), 7.51–7.42 (m, 1H), 7.13 (ddd, $J = 7.4, 4.8, 1.2$ Hz, 1H), 6.99 (ddd, $J = 9.2, 6.4, 1.0$ Hz, 1H), 6.78 (ddd, $J = 7.5, 6.4, 1.3$ Hz, 1H); ^{13}C NMR (151 MHz, Acetone- d_6) δ 156.29, 149.90, 138.68, 137.05, 131.28, 131.13, 131.06, 129.84, 129.62, 129.06, 123.10, 122.39, 122.16, 121.27, 120.22, 114.95.

2.1.2. Synthesis of 1,4-bis(1-(pyridin-2-yl)imidazo[1,5-*a*]pyridin-3-yl)benzene (**2**)

Derivative **2** was synthesized as previously reported [5] (yield 90%, 1.1 g). Mass (ESI) m/z calculated for $\text{C}_{30}\text{H}_{20}\text{N}_6$ ($[\text{M} + \text{H}]^+$): 465.17; found: 465.09: ^1H NMR (600 MHz, Chloroform- d): δ 8.74 (dt, $J = 9.2, 1.2$ Hz, 1H), 8.64 (ddd, $J = 4.9, 1.9, 0.9$ Hz, 1H), 8.34 (dt, $J = 7.2, 1.1$ Hz, 1H), 8.27 (dt, $J = 8.0, 1.1$ Hz, 1H), 8.05 (s, 2H), 7.76–7.72 (m, 1H), 7.14–7.08 (m, 1H), 6.96 (ddd, $J = 9.2, 6.3, 0.9$ Hz, 1H), 6.72 (ddd, $J = 7.5, 6.3, 1.3$ Hz, 1H); ^{13}C NMR (151 MHz, Chloroform- d): δ 155.08, 149.20, 137.51, 136.46, 131.17, 130.71, 130.55, 128.94, 122.17, 121.74, 121.45, 120.77, 120.15, 114.50.

2.1.3. Synthesis of 1,3-bis(1-(pyridin-2-yl)imidazo[1,5-*a*]pyridin-3-yl)benzene (**3**)

Derivative **3** was synthesized as previously reported [5] (yield 78%, 0.49 mg). Mass (ESI) m/z calculated for $\text{C}_{30}\text{H}_{20}\text{N}_6$ ($[\text{M} + \text{H}]^+$): 465.17; found: 465.23: ^1H NMR (600 MHz, Chloroform- d): δ 8.72 (dt, $J = 9.2, 1.2$ Hz, 1H), 8.63 (ddd, $J = 4.8, 1.8, 0.9$ Hz, 1H), 8.35–8.30 (m, 1.5H), 8.25 (dt, $J = 8.0, 1.1$ Hz, 1H), 7.93 (dd, $J = 7.7, 1.7$ Hz, 1H), 7.75–7.68 (m, 1.5H), 7.09 (ddd, $J = 7.4, 4.8, 1.2$ Hz, 1H), 6.94 (ddd, $J = 9.2, 6.4, 1.0$ Hz, 1H), 6.68 (ddd, $J = 7.4, 6.4, 1.3$ Hz, 1H); ^{13}C NMR (151 MHz, Chloroform- d): δ 155.03, 149.29, 149.12, 137.40, 136.38, 131.24, 130.94, 130.52, 129.89, 128.71, 128.37, 122.01, 121.70, 121.37, 120.66, 120.04, 114.37.

2.1.4. Synthesis of 1-ethyl-2-(3-phenylimidazo[1,5-*a*]pyridine-1-yl)pyridine-1-ium Iodide (**1q**)

In total, 70.6 mg (0.26 mmol) of **1** and 85 μL (1.04 mmol) of iodoethane were blended in a 5 mL vial in a microwave reactor with a molar ratio of 1:4. Then, 1 mL of acetonitrile was added. The reaction conditions were 155 °C for 50 min. The solution was clear and brown–yellow and, after the release of the pressure inside the reactor vial, a yellow precipitate formed spontaneously. The needle-shaped crystallites were washed several times with a petroleum ether:ethyl ether 3:1 mixture (yield: 48%, 53 mg). Mass (ESI) m/z calculated for $\text{C}_{20}\text{H}_{18}\text{N}_3$ ($[\text{M}]^+$): 300.15; found: 300.09. MS/MS: $m/z = 300.09$, loss of an ethyl group takes

place ($m/z = 272.06$): ^1H NMR (600 MHz, Acetone- d_6) δ 9.33 (ddd, $J = 6.4, 1.5, 0.6$ Hz, 1H), 8.77 (dt, $J = 7.2, 1.1$ Hz, 1H), 8.71 (ddd, $J = 8.1, 7.5, 1.5$ Hz, 1H), 8.53 (ddd, $J = 8.2, 1.5, 0.6$ Hz, 1H), 8.16 (dt, $J = 9.3, 1.2$ Hz, 1H), 8.14–8.04 (m, 1H), 8.04–7.98 (m, 2H), 7.66 (tt, $J = 6.9, 0.9$ Hz, 2H), 7.62–7.57 (m, 1H), 7.42 (ddd, $J = 9.2, 6.5, 1.0$ Hz, 1H), 7.14 (ddd, $J = 7.2, 6.5, 1.2$ Hz, 1H), 5.26 (q, $J = 7.2$ Hz, 2H), 1.77 (t, $J = 7.2$ Hz, 3H); ^{13}C NMR (151 MHz, Acetone- d_6) δ 148.29, 146.53, 144.99, 140.49, 134.36, 129.93, 129.41, 129.32, 129.02, 128.67, 126.08, 125.15, 124.04, 121.70, 117.61, 115.63, 54.92, 16.22.

2.1.5. Synthesis of 2,2'-(3,3'-(1,4-phenylene)bis(imidazo[1,5-*a*]pyridine-3,1-diyl))bis(1-ethylpyridin-1-ium iodide (2q))

In total, 189 mg (0.41 mmol) of **2** and 457 μL (5.6 mmol) of iodoethane were mixed in a 20 mL vial in a microwave reactor with a molar ratio of 1:14. Then, 10 mL of acetonitrile was added. The reaction conditions were 155 °C for 50 min. At the end of this process, the solution was red and a precipitate was present in the reactor vial. The powder was filtered and dried under vacuum. The solid was washed several times with an ether:ethyl ether 3:1 mixture (yield: 42%, 133 mg). Mass (ESI) m/z calculated for $\text{C}_{34}\text{H}_{30}\text{N}_6$ ($[\text{M}]^{++}$): 261.12; found: 261.33: ^1H NMR (600 MHz, Methanol- d_4) δ 9.01–8.97 (m, 1H), 8.81 (dt, $J = 7.2, 1.1$ Hz, 1H), 8.53 (td, $J = 7.9, 1.5$ Hz, 1H), 8.37 (dd, $J = 8.0, 1.4$ Hz, 1H), 8.21 (s, 2H), 8.03 (dt, $J = 9.2, 1.2$ Hz, 1H), 7.94 (ddd, $J = 7.8, 6.3, 1.5$ Hz, 1H), 7.41 (ddd, $J = 9.3, 6.5, 0.9$ Hz, 1H), 7.15–7.10 (m, 1H), 5.09 (q, $J = 7.1$ Hz, 2H), 1.73 (t, $J = 7.2$ Hz, 3H).

2.1.6. Synthesis of 2,2'-(3,3'-(1,3-phenylene)bis(imidazo[1,5-*a*]pyridine-3,1-diyl))bis(1-ethylpyridin-1-ium) iodide (3q))

In total, 363.5 mg (0.78 mmol) of **3** and 214 μL (2.6 mmol) of iodoethane were mixed in a 10 mL vial in a microwave reactor with a molar ratio of 1:8. Then, 5 mL of acetonitrile was added. The reaction conditions were 155 °C for 50 min. At the end of this process, the solution was red and a red precipitate was present in the vial. The powder was filtered and dried under vacuum. The solid was washed with a petroleum ether:ethyl ether 3:1 mixture several times (yield: 41%, 248 mg). Mass (ESI) m/z calculated for $\text{C}_{34}\text{H}_{30}\text{N}_6$ ($[\text{M}]^{++}$): 261.12; found: 261.17: ^1H NMR (600 MHz, Methanol- d_4) δ 8.95 (d, $J = 6.4$ Hz, 1H), 8.74 (d, $J = 7.2$ Hz, 1H), 8.48 (dd, $J = 15.3, 8.1$ Hz, 1.5H), 8.32 (d, $J = 7.7$ Hz, 1H), 8.14–8.06 (m, 1H), 8.02–7.81 (m, 2.5H), 7.36 (dd, $J = 9.1, 6.3$ Hz, 1H), 7.05 (t, $J = 6.9$ Hz, 1H), 5.03 (q, $J = 7.2$ Hz, 2H), 1.68 (t, $J = 7.1$ Hz, 3H).

2.2. Photophysical Properties

To avoid issues related with the presence of the halogen counter ion, which is well-known to quench the fluorescence intensity [35], the iodide was exchanged with hexafluorophosphate through an anion exchange resin, using an AmberLite ion exchange resin with ammonium hexafluorophosphate as the hexafluorophosphate source in the acetonitrile solution. ESI(-)/MS spectra confirmed the absence of an iodine anion ($m/z = 126.90$) and the presence of a hexafluorophosphate peak ($m/z = 144.96$).

Absorption spectra were recorded on a SHIMADZU UV/2600 spectrometer. The φ values were measured on an FS5 Spectrofluorometer with an integrating sphere SC-30 (Edinburgh Instruments, Livingston, UK). Excited state luminescence lifetimes were determined by Time-Correlated Single-Photon Counting (TCSPC); excitation was achieved with nanosecond pulses generated by pulsed diodes EPL-375 (372 nm). Emission decay data were collected in 2048 channels to 5000 counts in the peak channel and analyzed with the software Fluoracle® (TCSPC decay analysis software, Edinburgh Instruments, Livingston, UK). The average lifetime can be obtained by using the depicted formula reported in the literature [36]:

$$\langle \tau \rangle = \frac{A_1 \tau_1^2 + A_2 \tau_2^2}{A_1 \tau_1 + A_2 \tau_2} \quad (1)$$

Photophysical characterization was carried out both in solution (Dichloromethane, DCM) and in thin film.

Stock solutions with a concentration of 10 mg/mL in acetonitrile (**1** and **1q**), 1,2-dichloroethane (**2**) or tetrahydrofuran (**3**) were prepared for the thin films. The solutions were stirred in a closed vial at 50 °C for 1 h to achieve a clean solution. Compounds **2q** and **3q** were not tested in thin films due to their low solubility. The other two stock solutions of poly(methyl methacrylate) (PMMA) Mw 350,000 and polystyrene (PS) Mw 900,000 in acetonitrile with a concentration of 10 mg/mL were prepared and then blended with the fluorophore solutions in the desired ratio (%wt). Each blend was spin coated onto a quartz support at 1500 rpm for 30 s. The coated slides were then dried on a hot plate at 70 °C for 30 min. A spin coater, Model WS-650MZ23NPP (Laurell Technologies Corporation®, North Wales, PA, USA), was used.

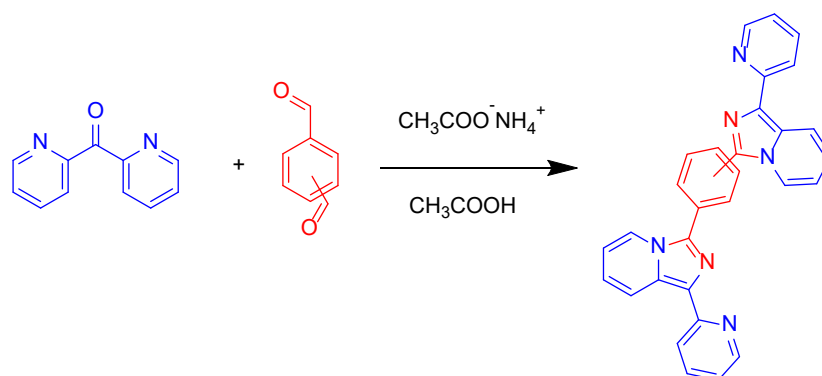
2.3. Computational Details

All calculations were performed with the Gaussian 09 program package (Gaussian, Inc., 2009, Wallingford, CT, USA) [37], employing the Density Functional Theory (DFT) and its Time-Dependent extension (TD-DFT) [38,39]. The Becke three-parameter hybrid functional [40], and the Lee–Yang–Parr’s gradient corrected correlation functional (B3LYP) [41] were used together with the 6–31G* basis set [42]. The solvent effect was included using the polarizable continuum model (CPCM method), with DCM as a solvent [43,44]. Geometry optimizations were carried out for ground states, without any symmetry constraints. The nature of all stationary points was verified via harmonic vibrational frequency calculations; no imaginary frequencies were found, indicating we had located minima on the potential energy surfaces. Electronic transitions were computed from the ground state as vertical excitation with linear response solvation by TD-DFT [38,39], employing the ground state optimized geometries. A total of twenty-four singlet excited states was computed for each compound, the electronic distribution and the localization of the singlet excited states were visualized using the Electron Density Difference Maps (EDDMs). GaussSum 2.2.5 was used to simulate the theoretical UV–Vis spectra and for EDDMs calculations [45,46]. Molecular graphic images were produced by using the UCSF Chimera package from the Resource for Biocomputing, Visualization, and Informatics at the University of California (San Francisco, CA, USA) [47].

3. Results and Discussion

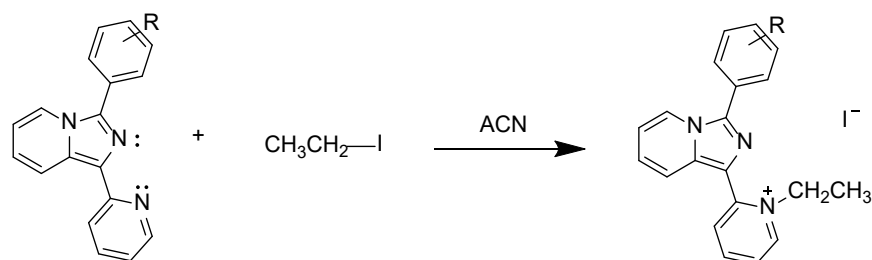
3.1. Note about the Synthesis

Compounds **1–3** were synthesized according to previously reported methods in the one-pot microwave-assisted protocol (Scheme 1) providing the products in yields over 80%.



Scheme 1. General reaction scheme of one-pot microwave-assisted cycloaddition used for **1–3**. Benzaldehyde, terephthalaldehyde and isophthalaldehyde were employed for **1–3**, respectively.

The quaternized salts **1q–3q** were prepared by a microwave-assisted S_N2 -type reaction starting from **1** to **3** and iodoethane in acetonitrile (Scheme 2).



Scheme 2. Scheme of the S_N2 -type reaction involved to obtain the desired pyridinium salts. The suitable lone pairs of the different heterocycles are explicit.

Although aromatic amines show the tendency to be less nucleophilic than secondary amines, they are still reactive with an excess of alkyl halides to be converted in quaternary ammonium salts [48]. In addition, pyridylimidazo[1,5-*a*]pyridines present two different sites able to promote a nucleophilic attack against the alkyl halide, namely the imidazolic N and the pyridinic N. Despite the numerous attempts, we could not grow suitable crystals for X-ray diffraction analysis of the products **1q–3q**. Therefore, to clarify the preferential reaction site, ^1H and ^{13}C NMR spectra were assigned with the help of the homonuclear correlation spectroscopy (COSY) method—Figure 2 and Figures S1–S4. Taking into account ^1H NMR, it is also noteworthy to mention that, in all the cases, the ratio between the aliphatic and aromatic regions inferred a reaction stoichiometry equal to 1:1 with respect to the pyridylimidazo[1,5-*a*]pyridine core and alkyl chain—Figures S2, S12 and S16. This first evidence also excludes a possible multi-quaternization step. Moreover, the pattern of the multiplets was retained upon quaternization, confirming that the reaction is selective toward only one of the suitable sites.

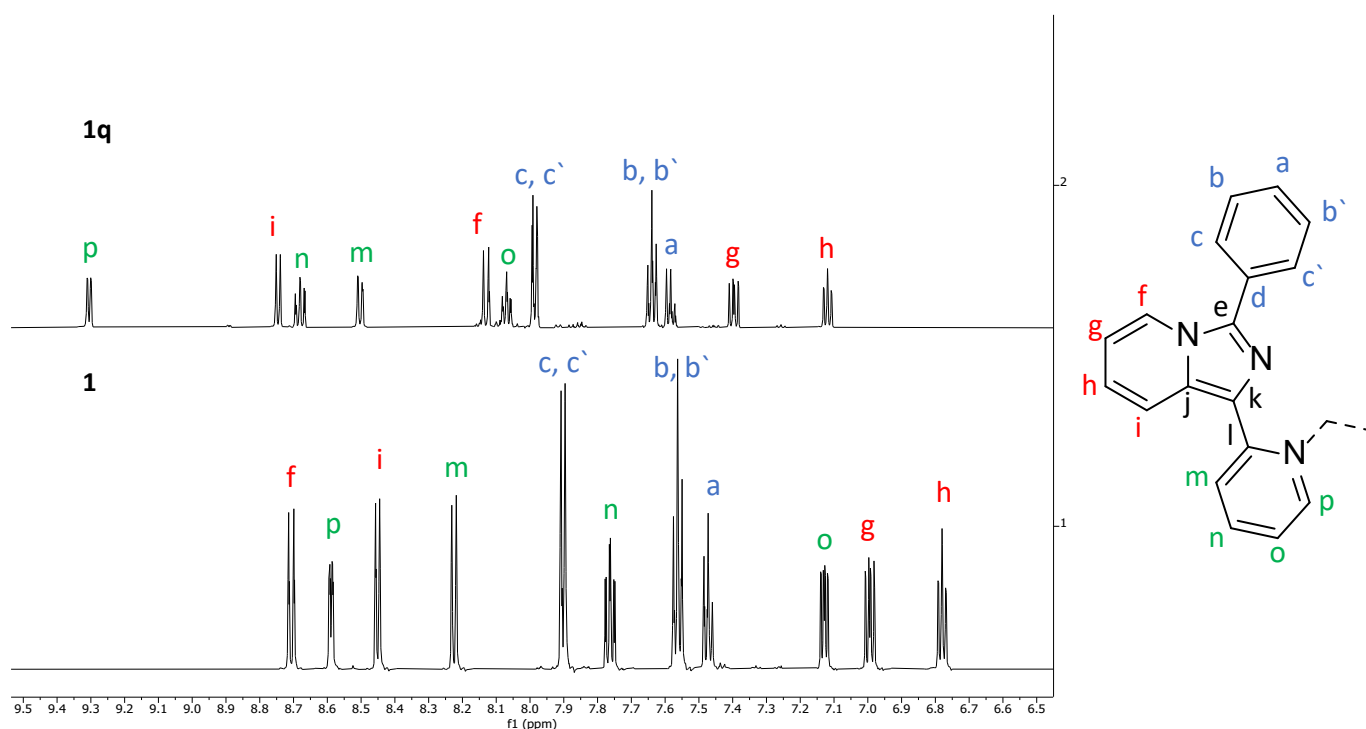


Figure 2. (Left): Aromatic region of the ^1H NMR spectra of **1** and **1q** (Acetone- d_6 solution). (Right): Atom labels.

The formation of a quaternary ammonium site shifted all the ^1H peaks, gathering an overall de-shielding of the aromatic moieties upon quaternization. Among others, the pyridinic ring suffered from the biggest de-shielding effect (almost 1 ppm). Further confirmation of this hypothesis is given by ^{13}C NMR. Close to the imidazolic N, two quaternary carbons are present, carbons e and k, while the pyridinic N is surrounded by one quaternary carbon and one ternary carbon, carbons l and p, respectively—Figure 2. Upon reaction with iodoethane, the ternary carbon p displayed the biggest shift in ^{13}C NMR—Figures S5 and S6. Final confirmation of the nature of the alkyl regions is given by the Distortionless Enhancement by Polarization Transfer (DEPT-135) analysis that correctly attributed the peak at δ 55.73 ppm to a $-\text{CH}_2-$ group—Figures S7 and S8.

Finally, we tried to replicate the quaternization reaction with 1,3-diphenylimidazo[1,5-*a*]pyridine as a substrate in the same conditions used for **1** and no product was obtained.

These evidences suggest the higher reactivity of pyridinic N when compared to the imidazolic N, with regard to the $\text{S}_{\text{N}}2$ -type reaction. Henceforth, the same considerations were expected to be valid for **2q** and **3q**—Figures S9–S16.

3.2. Notes about the Photophysical Properties

Since imidazo[1,5-*a*]pyridines are a well-established class of fluorophores, we investigated the effect of the quaternization reaction on the photophysical features [2,3,20,21,49]. The UV–Vis absorption spectrum of **1** in DCM displayed an intense high-energy band at 323 nm, together with a shoulder located at 380 nm. The fluorescence spectrum recorded upon excitation at 385 nm showed a blue emission, with a maximum located at 463 nm. The lifetime $\langle\tau\rangle$ associated to this excited state was 6.03 ns, inferring a fluorescence process. In addition, the ϕ in solution was 22%—Figure 3 and Table 1. Upon quaternization, both absorption and fluorescence spectra presented a remarkable bathochromic shift of almost 100 nm. More in detail, the UV–Vis absorption spectrum of **1q** in DCM showed a high-energy absorption band at 302 nm, followed by a second, more intense, absorption band located at 426 nm. Upon excitation at 425 nm, the recorded fluorescence spectrum of **1q** in the DCM solution showed a clear yellow emission at 551 nm. The $\langle\tau\rangle$ associated to this emission was 2.89 ns, confirming the fluorescence nature. Remarkably, the ϕ of **1q** in solution fell below 5%.

The drastic reduction of ϕ reported upon formation of pyridinium salts is in agreement with data reported for similar compounds [50]. Upon quaternization, the radiative decay constant (k_{rad}) of **1** decreased from $3.65 \times 10^7 \text{ s}^{-1}$ to $1.73 \times 10^7 \text{ s}^{-1}$ in **1q**, while the non-radiative constant followed the opposite trend—Table 1. Various possible mechanisms for intramolecular non-radiative relaxation of the S_1 states of pyridinium salts are possible, namely (i) intersystem crossing to the triplet state, (ii) reversible intramolecular electron-transfer proceeding to the ground state via the intermediate cation diradical, and (iii) rapid torsional relaxation, a mechanism found in intramolecular charge-transfer complexes of the molecular rotor type [51].

Table 1. Photophysical characterization in DCM solution (concentration 10^{-5} M) of the reported compounds.

Compound	$\lambda_{\text{abs}}/\text{nm}$	$\lambda_{\text{em}}/\text{nm}$	$\Delta\lambda_{\text{em-abs}}/\text{nm}$	$\phi/\%$	$\langle\tau\rangle/\text{ns}$	$k_{\text{rad}} 10^7/\text{s}^{-1}$	$k_{\text{nr}} 10^7/\text{s}^{-1}$
1	323	463	140	22	6.03	3.65	12.9
1q	302/426	551	125	<5	2.89	1.73	32.9
2	332/378	470	92	22	6.27	3.51	12.4
2q	303/353/425	524	99	<5	3.15	1.59	30.2
3	329	461	132	19	5.76	3.30	14.1
3q	316/430	515	85	<5	3.3	1.52	28.8

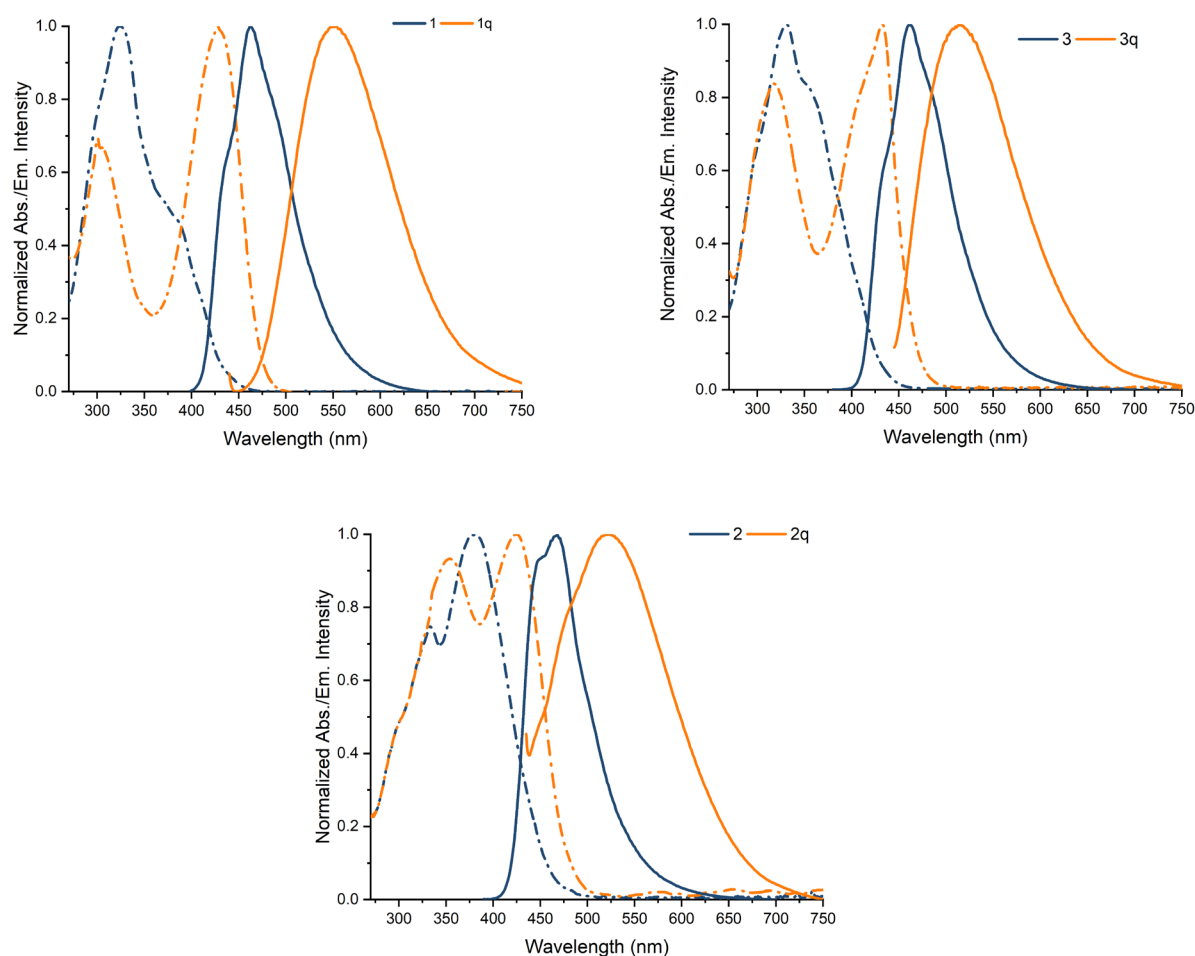


Figure 3. Absorption (dash–dotted lines) and emission (solid lines) spectra of **1**, **2**, **3** (blue) and **1q**, **2q**, **3q** (orange) recorded in DCM solution (concentration 10^{-5} M).

Further evidence of the quaternized pyridinic N is found from the contribution of Yagishita and collaborators [17]. The authors reported a remarkable blue shift related to a quaternization of imidazolic N in similar imidazo[1,5-*a*]pyridines compounds. The large bathochromic shift in the spectra of **1q** excludes the quaternization on the imidazolic N.

Similarly to **1**, the UV–Vis absorption spectra of **2** and **3** recorded in the DCM solution showed an initial high-energy shoulder located around 330 nm, followed by an intense absorption band centered at 378 nm and 360 nm, respectively. Upon excitation at 480 nm an intense blue emission around 465 nm was recorded in both cases. In addition, the ϕ in solution were found to be 22% and 19% for **2** and **3**—Figure 3 and Table 1. Interestingly, upon quaternization with iodoethane, both absorption and fluorescence spectra presented a less remarked bathochromic shift, around 50 nm, in comparison to **1**. In particular, the UV–Vis absorption spectrum of **2q** and **3q** in DCM showed a first high-energy absorption band at 350 nm, followed by a more intense absorption band located at 425 nm. Upon excitation at 425 nm, the recorded fluorescence spectra showed a clear green–yellow emission around 520 nm. The ϕ in solution in both cases was below 5%. The relative radiative and non-radiative constants followed the same trend described for **1** and **1q** systems—Table 1.

Importantly, the quaternization functionalization slightly reduced the Stokes shift, retaining a large value—i.e., >85 nm.

To shed light onto the structural, electronic, and optical properties of **1–3** and **1q–3q**, we performed a DFT and TD-DFT calculation at the B3LYP/6-31G* level, considering DCM as a solvent. The comparison of experimental and calculated absorption spectra showed good agreement along the series—Figure 4 and Figures S17–S20.

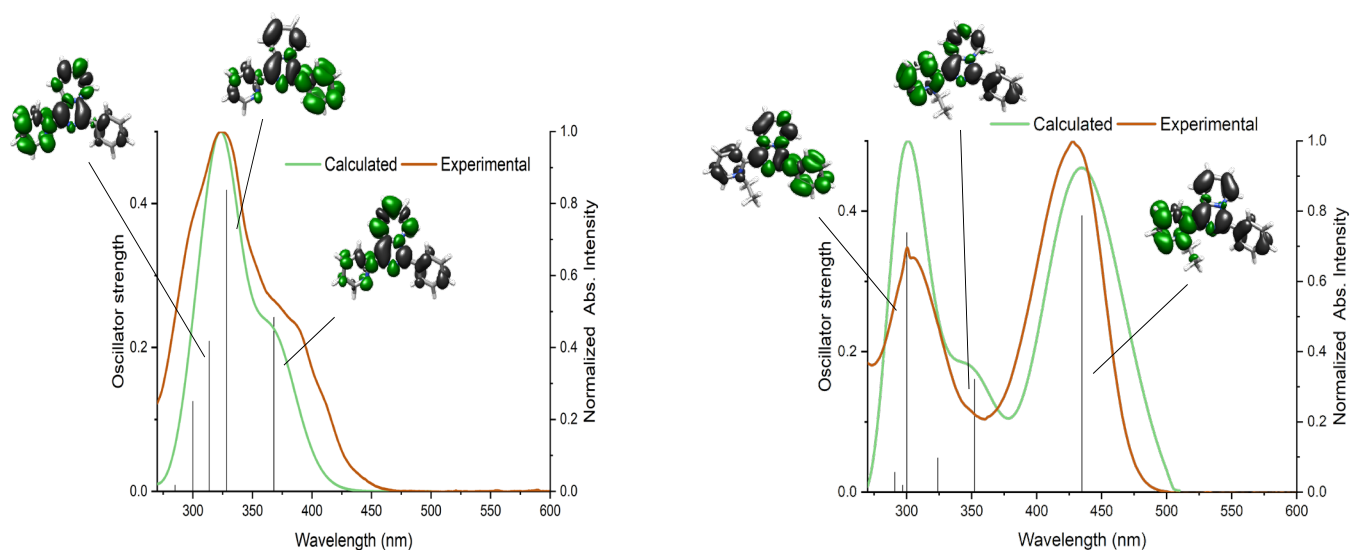


Figure 4. Experimental (orange) and calculated (green) absorption spectra of **1** (left) and **1q** (right). The Electron Density Difference Maps (EDDMs) of the most relevant transitions are shown.

The absorption of **1**, **2** and **3** originates mainly from the π - π^* and n - π^* electronic transitions, as confirmed from EDDMs. On the other hand, the absorption of **1q**, **2q** and **3q** is characterized by two clearly different electronics transitions. The low-energy band is related mainly with the HOMO–LUMO transition and displayed a strong charge transfer character, while the high-energy band is related with a π - π^* or n - π^* transition delocalized over the whole molecule. The charge transfer character was also confirmed by the lowering of the photoluminescence quantum yield, even in solution.

Secondly, the isodensity plots of the frontier molecular orbitals showed that HOMOs were delocalized over the whole molecule for all the reported compounds. On the other hand, the LUMOs were delocalized over the pyridylimidazo[1,5-*a*]pyridine moiety for **1**, **1q**, **2q**, **3** and **3q**. In the case of **2** also the LUMO was delocalized over the whole molecule. Remarkably, the introduction of a positive charge resulted in a huge stabilization effect, diminishing both HOMO and LUMO levels of almost 1 eV in all cases—Figure S21. The effect was stronger with regard to the LUMO level; hence; the final energy gap between the frontier orbitals was lower for the series **1q**, **2q** and **3q** with respect to the precursor, resulting in an emission at lower energy.

Taking into account also the lowering of the photoluminescence output, the reported functionalization led to promising acceptor small molecules.

Furthermore, we investigated the photophysical features of the fluorophores in thin films prepared by spin coating from an acetonitrile solution. Derivative **1**-based thin films presented almost no change in the absorption features in both the solution and thin films, while the fluorescence spectrum was remarkably different, with a substantial red shift of approximately 115 nm, along with a much broader emission covering all the spectrum from 450 to almost 800 nm—Figure S22 and Table 2. This is evidence that aggregation behavior concerns mainly the excited state, being related to an excimer-like emission. One of the methods to disrupt aggregates in both the ground and excited states involves the employment of a polymeric matrix. We selected PMMA and PS as polymeric matrices, since they are the most widely used in literature for thin film preparation [52,53]. The results obtained demonstrated that the aggregation behavior was reduced with both matrices. For instance, a 40 %wt of PMMA and PS diminished the red shift of the emission maximum from 115 nm to 80 nm and to 40, respectively, in **1**-based thin films—Figure 5. However, PMMA was scarcely effective as the emission of both monomer and excimer species were still present even when diluting **1** in a ratio of **1**:PMMA 25:75 %wt. Interestingly, the PS matrix significantly reduced the excimer emission already at **1**:PS 60:40 %wt dilution—Figure S23 and Table 2. Although the use of PS yielded to better results than those with

PMMA, further efforts are needed to diminish the amount of the insulating polymer matrix while retaining, or even increasing, the ϕ .

Table 2. Photophysical characterization of **1** and **1q** in pristine thin film or with different %wt of polymeric matrices.

Compound	Conditions	λ_{em}/nm	$\phi/\%$ (λ_{ex}/nm)	$\langle\tau\rangle/ns$	$k_{rad} 10^7/s^{-1}$	$k_{nrad} 10^7/s^{-1}$
1	Solution	463	22 (325)	6.03	3.65	12.9
	Thin film	613	<5 (330)	3.02	1.66	31.5
	25% PMMA	610	<5 (330)	1.96	2.55	48.5
	40% PMMA	507	<5 (330)	2.3	2.17	41.3
	75% PMMA	525	<5 (330)	2.23	2.24	42.6
	25% PS	612	<5 (330)	1.42	3.52	66.9
	40% PS	505	<5 (330)	1.93	2.59	49.2
	75% PS	502	<5 (330)	2.4	2.08	39.6
1q	Solution	550	<5 (420)	2.89	1.73	32.9
	Thin film	635	<5 (420)	1.87	2.67	50.8
	25% PS	635	<5 (420)	1.4	3.57	67.9
	40% PS	635	<5 (420)	1.17	4.27	81.2
	75% PS	635	<5 (420)	1.36	3.68	69.9

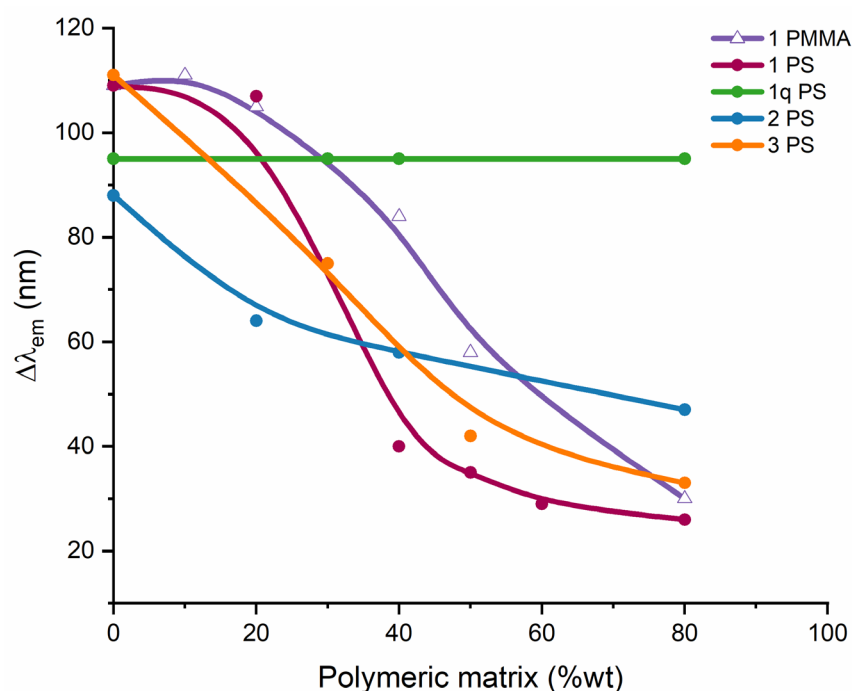


Figure 5. Difference of the emission maximum in thin film and the one in solution ($\Delta\lambda_{em}$) vs. %wt of polymeric matrix. See legend.

Noteworthy, the red shift in the emission spectrum displayed by **1q** with regard to **1** was further increased in the thin films (100 nm). By contrast, the addition of the aforementioned polymeric matrices did not display a remarkable effect on the absorption and emission features, inferring the lack of π - π type aggregates—Figure S24 and Table 2.

Similarly, **2** and **3** presented no change of their absorption features in both solution and thin films, while the fluorescence spectra were affected by aggregation phenomena—Figures S25 and S26 and Table S1. They both showed a broadened emission spectrum,

peaking at 550 nm and 572 nm for **2** and **3**, respectively. In both cases, two clearly different emissive states were not present. It is plausible that the presence of a second pyridylimidazo[1,5-*a*]pyridine moiety allowed the assembly of supramolecular aggregates with a broader emission. Nevertheless, the evidence of a possible aggregation behavior was indicated by the huge red shift (more than 110 nm) between fluorescence in solution and emission in thin film. Furthermore, the featured emission red shift gradually decreased with the increasing of the mass ratio of the polymeric matrix (Figure 5). Moreover, for **2** and **3**, the PS matrix turned out to be effective in reducing the aggregating issues—Figures S25 and S26 and Table S1. Indeed, a 50 %wt of PS was sufficient for both compounds to show no relevant aggregation feature and a red shift of 60 nm and 40 nm compared to the spectrum in the solutions of **2** and **3**, respectively. Remarkably, the ϕ values were below 5% in each case in the solid state. Both the red shift and the lowered ϕ indicate the presence of an efficient quenching process.

4. Conclusions

To summarize, in this contribution we synthesized and characterized new members of the promising family of pyridylimidazo[1,5-*a*]pyridine: **1q**, **2q** and **3q**. First, we investigated the preferential reaction site through an in-depth NMR spectroscopic analysis. Noteworthy, the presence of a second suitable site for quaternization led to a drastic change in the reactivity of the substrates, namely the pyridinic heteroatom was the preferential reaction site in all the considered cases. In addition, **1q–3q** featured a lower energetic emission and absorption (90 nm shift) compared to those of **1–3** in solution, characterized by a strong additional charge transfer transition, as confirmed by DFT calculations. Remarkably, the reported computational studies highlight that the introduction of a positive charge on the pyridylimidazo[1,5-*a*]pyridine unit resulted in a huge stabilization effect, lowering both HOMO and LUMO levels. Secondly, we turned our attention to thin film applications with a detailed photophysical characterization. In this context, it is noteworthy to mention that the aggregation tendency of **1–3** and **1q** in thin film was rationalized, pointing out that the introduction of a second imidazo[1,5-*a*]pyridine in position meta (**3**) was more effective in reducing aggregates with respect to the para position (**2**). Encouraging results were also obtained with the aid of polymeric matrices for thin films, as 40–50 %wt of PS was proven to completely cancel the aggregation features. In addition, the quaternized derivatives featured a strong stabilization of HOMO–LUMO energy levels, i.e., -5.18 eV / -1.80 eV and -6.03 eV / -3.17 eV for **1** and **1q**, respectively.

Overall, this work relates on a series of pyridylimidazo[1,5-*a*]pyridines and its corresponding quaternized salts and provides relevant information with respect to the reactivity with haloalkanes and the photophysical properties in both solution and thin films for the pristine compounds and in polymeric matrices. We provide two most relevant results. First, the very low-lying energy levels reached through the quaternization reaction make them promising candidates as a charged molecular acceptor constituent in future exciplex-based host–guest blends. Secondly, this study paves the way for possible future studies focused on position 3 on the imidazo[1,5-*a*]pyridines core, in order to improve the optical properties-avoiding aggregation process in the solid state, as here demonstrated.

Based on the reported promising properties, further studies are in progress to test these derivatives as tunable low-cost fluorescent materials for down-conversion and optoelectronic devices.

Supplementary Materials: The following are available online at <https://www.mdpi.com/article/10.3390/chemistry3030050/s1>, Figure S1: the ^1H NMR spectrum of Acetone- d_6 solution of **1**, Figure S2: the ^1H NMR spectrum of Acetone- d_6 solution of **1q**, Figure S3: the 2D ^1H -COSY NMR spectrum of Acetone- d_6 solution of **1**, Figure S4: the 2D ^1H -COSY NMR spectrum of Acetone- d_6 solution of **1q**, Figure S5: the ^{13}C NMR spectrum of Acetone- d_6 solution of **1**, Figure S6: the ^{13}C NMR spectrum of Acetone- d_6 solution of **1q**, Figure S7: the ^{13}C DEPT-135 NMR spectrum of Acetone- d_6 solution of **1**, Figure S8: the ^{13}C DEPT-135 NMR spectrum of Acetone- d_6 solution of **1q**, Figure S9: the ^1H NMR spectrum of Chloroform- d_3 solution of **2**, Figure S10: the 2D ^1H COSY-NMR spectrum of

Chloroform-d₃ solution of 2, Figure S11: the ¹³C NMR spectrum of Chloroform-d₃ solution of 2, Figure S12: the ¹H NMR spectrum of Methanol-d₄ solution of 2q, Figure S13: the ¹H NMR spectrum of Chloroform-d₃ solution of 3, Figure S14: the 2D ¹H COSY-NMR spectrum of Chloroform-d₃ solution of 3, Figure S15: the ¹³C NMR spectrum of Chloroform-d₃ solution of 3, Figure S16: the ¹H NMR spectrum of Methanol-d₄ solution of 3q, Figure S17: experimental and calculated absorption spectra of 2, Figure S18: experimental and calculated absorption spectra of 2q, Figure S19: experimental and calculated absorption spectra of 3, Figure S20: experimental and calculated absorption spectra of 3q, Figure S21: molecular orbital plots (LUMO and HOMO) of the reported compounds, Figure S22: absorption and emission spectra of 1 recorded in DCM solution (concentration 10⁻⁵ M) and in thin film, Figure S23: emission spectra of 1 recorded in different conditions: DCM solution, thin film, and blended in PMMA and in PS, Figure S24: absorption and emission spectra of 1q recorded in DCM solution (concentration 10⁻⁵ M), in thin film and blended in PS matrix, Figure S25: absorption and emission spectra of 2 recorded in DCM solution (concentration 10⁻⁵ M), in thin film and blended in PS matrix, Figure S26: absorption and emission spectra of 3 recorded in DCM solution (concentration 10⁻⁵ M), in thin film and blended in PS matrix.

Author Contributions: Conceptualization, G.V. and L.M.C.; formal analysis, E.F. and L.M.C.; investigation, L.M.C. and E.F.; data curation, C.G.; methodology, A.F. and C.G.; writing—original draft preparation, L.M.C.; supervision, G.V.; writing—review and editing, C.G., A.F. and G.V.; funding acquisition, C.B.; resources, C.B. All authors have read and agreed to the published version of the manuscript.

Funding: This research received no external funding.

Institutional Review Board Statement: Not applicable.

Informed Consent Statement: Not applicable.

Data Availability Statement: Not applicable.

Conflicts of Interest: The authors declare no conflict of interest.

References

1. Volpi, G.; Magnano, G.; Benesperi, I.; Saccone, D.; Priola, E.; Gianotti, V.; Milanesio, M.; Conterosito, E.; Barolo, C.; Viscardi, G. One pot synthesis of low cost emitters with large Stokes' shift. *Dye. Pigment.* **2017**, *137*, 152–164. [[CrossRef](#)]
2. Volpi, G.; Lace, B.; Garino, C.; Priola, E.; Artuso, E.; Cerreia Vioglio, P.; Barolo, C.; Fin, A.; Genre, A.; Prandi, C. New substituted imidazo[1,5-a]pyridine and imidazo[5,1-a]isoquinoline derivatives and their application in fluorescence cell imaging. *Dye. Pigment.* **2018**, *157*, 298–304. [[CrossRef](#)]
3. Volpi, G.; Rabezzana, R. Imidazo[1,5-a]pyridine derivatives: Useful, luminescent and versatile scaffolds for different applications. *New J. Chem.* **2021**, *45*, 5737–5743. [[CrossRef](#)]
4. Volpi, G.; Garino, C.; Fresta, E.; Casamassa, E.; Giordano, M.; Barolo, C.; Viscardi, G. Strategies to increase the quantum yield: Luminescent methoxylated imidazo[1,5-a]pyridines. *Dye. Pigment.* **2021**, *192*, 109455. [[CrossRef](#)]
5. Volpi, G.; Garino, C.; Conterosito, E.; Barolo, C.; Gobetto, R.; Viscardi, G. Facile synthesis of novel blue light and large Stoke shift emitting tetradentate polyazines based on imidazo[1,5-a]pyridine. *Dye. Pigment.* **2016**, *128*, 96–100. [[CrossRef](#)]
6. Volpi, G.; Garino, C.; Priola, E.; Diana, E.; Gobetto, R.; Buscaino, R.; Viscardi, G.; Barolo, C. Facile synthesis of novel blue light and large Stoke shift emitting tetradentate polyazines based on imidazo[1,5- a]pyridine—Part 2. *Dye. Pigment.* **2017**, *143*, 284–290. [[CrossRef](#)]
7. Blanco-Rodríguez, A.M.; Kvapilová, H.; Sýkora, J.; Towrie, M.; Nervi, C.; Volpi, G.; Zalis, S.; Vlček, A. Photophysics of Singlet and Triplet Intraligand Excited States in [ReCl(CO)3(1-(2-pyridyl)-imidazo[1,5- α]pyridine)] Complexes. *J. Am. Chem. Soc.* **2014**, *136*, 5963–5973. [[CrossRef](#)]
8. Garino, C.; Ruiui, T.; Salassa, L.; Albertino, A.; Volpi, G.; Nervi, C.; Gobetto, R.; Hardcastle, K.I. Spectroscopic and Computational Study on New Blue Emitting ReL(CO)3Cl Complexes Containing Pyridylimidazo[1,5-a]pyridine Ligands. *Eur. J. Inorg. Chem.* **2008**, *2008*, 3587–3591. [[CrossRef](#)]
9. Volpi, G.; Priola, E.; Garino, C.; Daolio, A.; Rabezzana, R.; Benzi, P.; Giordana, A.; Diana, E.; Gobetto, R. Blue fluorescent zinc(II) complexes based on tunable imidazo[1,5-a]pyridines. *Inorganica Chim. Acta* **2020**, *509*, 119662. [[CrossRef](#)]
10. Chen, F.; Liu, A.; Ji, R.; Xu, Z.; Dong, J.; Ge, Y. A FRET-based probe for detection of the endogenous SO₂ in cells. *Dye. Pigment.* **2019**, *165*, 212–216. [[CrossRef](#)]
11. Denora, N.; Lee, C.; Iacobazzi, R.M.; Choi, J.Y.; Song, I.H.; Yoo, J.S.; Piao, Y.; Lopalco, A.; Leonetti, F.; Lee, B.C.; et al. TSPO-targeted NIR-fluorescent ultra-small iron oxide nanoparticles for glioblastoma imaging. *Eur. J. Pharm. Sci.* **2019**, *139*, 105047. [[CrossRef](#)] [[PubMed](#)]

12. Song, G.-J.; Bai, S.-Y.; Dai, X.; Cao, X.-Q.; Zhao, B.-X. A ratiometric lysosomal pH probe based on the imidazo[1,5-a]pyridine–rhodamine FRET and ICT system. *RSC Adv.* **2016**, *6*, 41317–41322. [[CrossRef](#)]
13. Priyanga, S.; Khamrang, T.; Velusamy, M.; Karthi, S.; AshokKumar, B.; Mayilmurugan, R.; Selvarasu, P.; Ramasamy, M. Coordination geometry-induced optical imaging of l-cysteine in cancer cells using imidazopyridine-based copper(ii) complexes. *Dalton Trans.* **2019**, *48*, 1489–1503. [[CrossRef](#)]
14. Vanda, D.; Zajdel, P.; Soural, M. Imidazopyridine-based selective and multifunctional ligands of biological targets associated with psychiatric and neurodegenerative diseases. *Eur. J. Med. Chem.* **2019**, *181*, 111569. [[CrossRef](#)] [[PubMed](#)]
15. Hutt, J.T.; Jo, J.; Olasz, A.; Chen, C.-H.; Lee, N.; Aron, Z.D. Fluorescence Switching of Imidazo[1,5-a]pyridinium Ions: pH-Sensors with Dual Emission Pathways. *Org. Lett.* **2012**, *14*, 3162–3165. [[CrossRef](#)]
16. Hutt, J.T.; Aron, Z.D. Synthesis and Application of Ratiometric and “Turn-On” Fluorescent pH Sensors: An Advanced Organic Undergraduate Laboratory. *J. Chem. Educ.* **2014**, *91*, 1990–1994. [[CrossRef](#)]
17. Yagishita, F.; Tanigawa, J.-I.; Nii, C.; Tabata, A.; Nagamune, H.; Takanari, H.; Imada, Y.; Kawamura, Y.; Tanigawa, J.-I. Fluorescent Imidazo[1,5-a]pyridinium Salt for a Potential Cancer Therapy Agent. *ACS Med. Chem. Lett.* **2019**, *10*, 1110–1114. [[CrossRef](#)] [[PubMed](#)]
18. Yagishita, F.; Nii, C.; Tezuka, Y.; Tabata, A.; Nagamune, H.; Uemura, N.; Yoshida, Y.; Mino, T.; Sakamoto, M.; Kawamura, Y. Fluorescent N-Heteroarenes Having Large Stokes Shift and Water Solubility Suitable for Bioimaging. *Asian J. Org. Chem.* **2018**, *7*, 1614–1619. [[CrossRef](#)]
19. Santoro, A.; Lord, R.M.; Loughrey, J.J.; McGowan, P.C.; Halcrow, M.A.; Henwood, A.F.; Thomson, C.; Zysman-Colman, E. One-Pot Synthesis of Highly Emissive Dipyridinium Dihydrohelicenes. *Chem. A Eur. J.* **2015**, *21*, 7035–7038. [[CrossRef](#)]
20. Albrecht, G.; Geis, C.; Herr, J.; Ruhl, J.; Göttlich, R.; Schlettwein, D. Electroluminescence and contact formation of 1-(pyridin-2-yl)-3-(quinolin-2-yl)imidazo[1,5-a]quinoline thin films. *Org. Electron.* **2019**, *65*, 321–326. [[CrossRef](#)]
21. Albrecht, G.; Rössiger, C.; Herr, J.M.; Locke, H.; Yanagi, H.; Göttlich, R.; Schlettwein, D. Optimization of the Substitution Pattern of 1,3-Disubstituted Imidazo[1,5-a]Pyridines and -Quinolines for Electro-Optical Applications. *Phys. Status Solid.* **2020**, *257*, 1900677. [[CrossRef](#)]
22. Fresta, E.; Volpi, G.; Garino, C.; Barolo, C.; Costa, R.D. Contextualizing yellow light-emitting electrochemical cells based on a blue-emitting imidazo-pyridine emitter. *Polyhedron* **2018**, *140*, 129–137. [[CrossRef](#)]
23. Weber, M.D.; Garino, C.; Volpi, G.; Casamassa, E.; Milanesio, M.; Barolo, C.; Costa, R.D. Origin of a counterintuitive yellow light-emitting electrochemical cell based on a blue-emitting heteroleptic copper(i) complex. *Dalton Trans.* **2016**, *45*, 8984–8993. [[CrossRef](#)]
24. Pashaei, B.; Karimi, S.; Shahroosvand, H.; Abbasi, P.; Pilkington, M.; Bartolotta, A.; Fresta, E.; Fernandez-Cestau, J.; Costa, R.D.; Bonaccorso, F. Polypyridyl ligands as a versatile platform for solid-state light-emitting devices. *Chem. Soc. Rev.* **2019**, *48*, 5033–5139. [[CrossRef](#)] [[PubMed](#)]
25. Keller, S.; Brunner, F.; Junquera-Hernández, J.M.; Pertegás, A.; La-Placa, M.-G.; Prescimone, A.; Constable, E.C.; Bolink, H.J.; Ortí, E.; Housecroft, C.E. CF₃ Substitution of [Cu(P[∞]P)(bpy)][PF₆][−] Complexes: Effects on Photophysical Properties and Light-Emitting Electrochemical Cell Performance. *ChemPlusChem* **2018**, *83*, 217–229. [[CrossRef](#)] [[PubMed](#)]
26. Arnosti, N.; Brunner, F.; Susic, I.; Keller, S.; Junquera-Hernández, J.M.; Prescimone, A.; Bolink, H.J.; Sessolo, M.; Ortí, E.; Housecroft, C.E.; et al. Remote Modification of Bidentate Phosphane Ligands Controlling the Photonic Properties in Their Complexes: Enhanced Performance of [Cu(RN-xantphos)(N[∞]N)][PF₆][−] in Light-Emitting Electrochemical Cells. *Adv. Opt. Mater.* **2020**, *8*, 1901689. [[CrossRef](#)]
27. Keller, S.; Prescimone, A.; Bolink, H.J.; Sessolo, M.; Longo, G.; Martínez-Sarti, L.; Junquera-Hernandez, J.M.; Constable, E.C.; Ortí, E.; Housecroft, C.E. Luminescent copper(i) complexes with bisphosphane and halogen-substituted 2,2'-bipyridine ligands. *Dalton Trans.* **2018**, *47*, 14263–14276. [[CrossRef](#)] [[PubMed](#)]
28. Shanmugasundaram, K.; Subeesh, M.S.; Sunesh, C.D.; Choe, Y. Non-doped deep blue light-emitting electrochemical cells from charged organic small molecules. *RSC Adv.* **2016**, *6*, 28912–28918. [[CrossRef](#)]
29. Gong, X.; Ostrowski, J.; Moses, D.; Bazan, G.; Heeger, A. Electrophosphorescence from a Polymer Guest–Host System with an Iridium Complex as Guest: Förster Energy Transfer and Charge Trapping. *Adv. Funct. Mater.* **2003**, *13*, 439–444. [[CrossRef](#)]
30. Wong, Y.; Hedley, G.; Xie, G.; Kölln, L.S.; Samuel, I.; Pertegás, A.; Bolink, H.; Zysman-Colman, E. Light-Emitting Electrochemical Cells and Solution-Processed Organic Light-Emitting Diodes Using Small Molecule Organic Thermally Activated Delayed Fluorescence Emitters. *Chem. Mater.* **2015**, *27*, 6535–6542. [[CrossRef](#)]
31. Chen, H.-F.; Liao, C.-T.; Su, H.-C.; Yeh, Y.-S.; Wong, K.-T. Highly efficient exciplex emission in solid-state light-emitting electrochemical cells based on mixed ionic hole-transport triarylamine and ionic electron-transport 1,3,5-triazine derivatives. *J. Mater. Chem. C* **2013**, *1*, 4647–4654. [[CrossRef](#)]
32. Shanmugasundaram, K.; Subeesh, M.S.; Sunesh, C.D.; Chitumalla, R.K.; Jang, J.; Choe, Y. Green Electroluminescence from Charged Phenothiazine Derivative. *J. Phys. Chem. C* **2016**, *120*, 20247–20253. [[CrossRef](#)]
33. Vassilyeva, O.Y.; Buvaylo, E.A.; Lobko, Y.V.; Linnik, R.P.; Kokozay, V.N.; Skelton, B.W. Organic–inorganic hybrid tetrachlorocadmates as promising fluorescent agents for cross-linked polyurethanes: Synthesis, crystal structures and extended performance analysis. *RSC Adv.* **2021**, *11*, 7713–7722. [[CrossRef](#)]

34. Salassa, L.; Garino, C.; Albertino, A.; Volpi, G.; Nervi, C.; Gobetto, R.; Hardcastle, K.I. Computational and Spectroscopic Studies of New Rhenium(I) Complexes Containing Pyridylimidazo[1,5-a]pyridine Ligands: Charge Transfer and Dual Emission by Fine-Tuning of Excited States. *Organometallics* **2008**, *27*, 1427–1435. [[CrossRef](#)]
35. Chmyrov, A.; Sandén, T.; Widengren, J. Iodide as a Fluorescence Quencher and Promoter—Mechanisms and Possible Implications. *J. Phys. Chem. B* **2010**, *114*, 11282–11291. [[CrossRef](#)]
36. Luk, C.M.; Tang, L.B.; Teng, K.S.; Lau, S.P.; Zhang, W.F.; Yu, S.F. An efficient and stable fluorescent graphene quantum dot–agar composite as a converting material in white light emitting diodes. *J. Mater. Chem.* **2012**, *22*, 22378–22381. [[CrossRef](#)]
37. Frisch, M.J.; Trucks, G.W.; Schlegel, H.B.; Scuseria, G.E.; Robb, M.A.; Cheeseman, J.R.; Scalmani, G.; Barone, V.; Petersson, G.A.; Nakatsuji, H.; et al. *Gaussian 16*; Gaussian Inc.: Wallingford, CT, USA, 2016.
38. Stratmann, R.E.; Scuseria, G.E.; Frisch, M.J. An efficient implementation of time-dependent density-functional theory for the calculation of excitation energies of large molecules. *J. Chem. Phys.* **1998**, *109*, 8218–8224. [[CrossRef](#)]
39. Casida, M.E.; Jamorski, C.J.; Casida, K.C.; Salahub, D.R. Molecular excitation energies to high-lying bound states from time-dependent density-functional response theory: Characterization and correction of the time-dependent local density approximation ionization threshold. *J. Chem. Phys.* **1998**, *108*, 4439–4449. [[CrossRef](#)]
40. Becke, A.D. Density-functional thermochemistry. III. The role of exact exchange. *J. Chem. Phys.* **1993**, *98*, 5648–5652. [[CrossRef](#)]
41. Lee, C.; Yang, W.; Parr, R.G. Development of the Colle-Salvetti correlation-energy formula into a functional of the electron density. *Phys. Rev. B* **1988**, *37*, 785–789. [[CrossRef](#)]
42. McLean, A.D.; Chandler, G.S. Contracted Gaussian basis sets for molecular calculations. I. Second row atoms, Z=11–18. *J. Chem. Phys.* **1980**, *72*, 5639–5648. [[CrossRef](#)]
43. Miertus, S.; Scrocco, E.; Tomasi, J. Electrostatic interaction of a solute with a continuum. A direct utilization of AB initio molecular potentials for the prevision of solvent effects. *Chem. Phys.* **1981**, *55*, 117–129. [[CrossRef](#)]
44. Cossi, M.; Scalmani, G.; Rega, N.; Barone, V. New developments in the polarizable continuum model for quantum mechanical and classical calculations on molecules in solution. *J. Chem. Phys.* **2002**, *117*, 43–54. [[CrossRef](#)]
45. Browne, W.R.; O’Boyle, N.M.; McGarvey, J.J.; Vos, J.G. Elucidating excited state electronic structure and intercomponent interactions in multicomponent and supramolecular systems. *Chem. Soc. Rev.* **2005**, *34*, 641–663. [[CrossRef](#)]
46. Head-Gordon, M.; Grana, A.; Maurice, D.; White, C.A. Analysis of Electronic Transitions as the Difference of Electron Attachment and Detachment Densities. *J. Phys. Chem.* **1995**, *99*, 14261–14270. [[CrossRef](#)]
47. Pettersen, E.F.; Goddard, T.D.; Huang, C.C.; Couch, G.S.; Greenblatt, D.M.; Meng, E.C.; Ferrin, T.E. UCSF Chimera—A visualization system for exploratory research and analysis. *J. Comput. Chem.* **2004**, *25*, 1605–1612. [[CrossRef](#)] [[PubMed](#)]
48. Westheimer, F.H.; Taguchi, K. Catalysis by molecular sieves in the preparation of ketimines and enamines. *J. Org. Chem.* **1971**, *36*, 1570–1572. [[CrossRef](#)]
49. Albrecht, G.; Herr, J.; Steinbach, M.; Yanagi, H.; Göttlich, R.; Schlettwein, D. Synthesis, optical characterization and thin film preparation of 1-(pyridin-2-yl)-3-(quinolin-2-yl)imidazo[1,5-a]quinoline. *Dye. Pigment.* **2018**, *158*, 334–341. [[CrossRef](#)]
50. Skalski, B.; Paszyc, S.; Adamiak, R.W.; Steer, R.P.; Verrall, R.E. Photophysical properties of pyridinium salts derived from purine bases. *Can. J. Chem.* **1990**, *68*, 2164–2170. [[CrossRef](#)]
51. Abdel-Mottaleb, M.S.A.; Loutfy, R.O.; Lapouyade, R. Non-radiative deactivation channels of molecular rotors. *J. Photochem. Photobiol. A Chem.* **1989**, *48*, 87–93. [[CrossRef](#)]
52. Fresta, E.; Dosso, J.; Cabanillas-González, J.; Bonifazi, D.; Costa, R.D. Origin of the Exclusive Ternary Electroluminescent Behavior of BN-Doped Nanographenes in Efficient Single-Component White Light-Emitting Electrochemical Cells. *Adv. Funct. Mater.* **2020**, *30*, 1906830. [[CrossRef](#)]
53. Fresta, E.; Dosso, J.; Cabanillas-Gonzalez, J.; Bonifazi, D.; Costa, R.D. Revealing the Impact of Heat Generation Using Nanographene-Based Light-Emitting Electrochemical Cells. *ACS Appl. Mater. Interf.* **2020**, *12*, 28426–28434. [[CrossRef](#)] [[PubMed](#)]